Journal of Computing and Electronic Information Management
ISSN: 2413-1660 | Vol. 13, No. 1, 2024

Dual-band microwave sensor based on cross-finger MCSRR Research

Danni Gao

School of Electronic Information, Southwest Minzu University, Chengdu, China

Abstract: This paper presents a low-cost, easy-to-fabricate microwave resonant sensor for characterising the dielectric properties of solids. The designed sensor is based on a Rogers RT/duriod 5880 substrate with a cross-finger treated Multiple Complementary Split-Ring Resonator (MCSRR) structure etched on it, and this resonance unit is used to place the Material Under Test (MUT). The sensor operates at 5.8 GHz and 8.3 GHz resonant frequencies and uses offset resonance to detect the dielectric properties of different solids. The relationships established by the simulation were experimentally verified by the fabricated sensor. The percentage error between the calculated dielectric constant and the reference dielectric constant is less than 9.58% for a certain thickness of the sample to be tested, which verifies the feasibility of the proposed loaded cross-finger MCSRR sensor. Therefore, this sensor is expected to be a cost-effective and convenient solution.

Keywords: Commas; Microwave sensors; Multiple Complementary Split-Ring Resonator (MCSRR); Dielectric constant.

1. Introduction

Industrial Scientific Medical Band is a band that is open for use by three main organisations: industrial, scientific and medical. Typical operating frequencies in the microwave band are 2.45 GHz and 5.8 GHz, while the 5.8 GHz band is a higher frequency than the 2.4 GHz, open ISM band and is expected to replace 2.4 GHz wireless technology technology. With the deepening development of the modern communication field, the wide application of RF microwave technology has increasingly highlighted the demand for sensors with miniaturised and integrated characteristics, and new materials, new processes and advanced manufacturing skills continue to emerge to provide support for the performance enhancement and cost reduction of RF microwave measurements, and the design of microwave resonance sensors with higher sensitivity and smaller dimensions has become one of the hot spots of research for scholars both at home and abroad.

The concept of left-handed materials was first proposed by V. G. Veselago in the 1960s. [1] Its theoretical study is based on Maxell Equations. In the field of electromagnetism, the electromagnetic properties of dielectric materials have always been described by the two main parameters of dielectric constant ε and magnetic permeability μ . Based on the Maxell Equations, V. G. Veselago discussed in detail what happens to dielectric materials with different combinations of dielectric constant ε and magnetic permeability μ (negative-positive, positive-positive, negative-negative, and positive-negative), and showed that Maxell Equations hold for all the four cases. is valid in all four cases. However, due to the unknown nature of such materials in nature, the study of left-handed materials failed to make significant progress for quite some time. It was not until around 1996 that scholars such as J. B. Pendry and others proposed in their papers a periodically arranged array of fine metallic wires that exhibited a negative equivalent permittivity[2] . Subsequently, scholars discovered periodic arrays consisting of Split-Ring Resonator (SRR), whose equivalent permeability was also negative. In the 21st century, D. R. Smith et al. successfully proposed the left-handed material, an artificial dielectric material with negative values of dielectric constant ε and magnetic permeability μ , based on the previous research, thus bringing the research on left-handed materials to a new level.[3] The research on left-handed materials has been pushed from theory to reality.[4-8] In 2004, F. Falcone et al. designed a complementary structure to the SRR structure, called CSRR, to address the unique properties of the SRR structure.[9] The CSRR is a left-handed material. As a left-handed material, the CSRR structure is not only simple to design and structure, but also easy to fabricate, which makes it excellent for microwave applications such as antennas, filters, sensors, and power dividers.[10] These characteristics make them excellent in microwave applications such as antennas, filters, sensors, and power dividers, and provide a good solution for the design and research of new microwave devices.

Through the joint efforts of researchers at home and abroad, the subject based on CSRR structure becomes more and more perfect and mature. At present, CSRR-based sensors are widely used in such fields as displacement detection [13-17], dielectric detection [18-22] and gas-sensitive detection [23-25]. Microwave sensors based on CSRR structure are characterised by smaller physical size, easy integration, higher measurement accuracy and relatively simple data processing. The above features significantly reduce the measurement cost of microwave resonant sensors, and the requirements for the measurement environment are significantly reduced. In addition, these features simplify the entire measurement process by reducing the tedious preliminary preparation work [26-32].

Based on this, this paper proposes a Multiple Complementary Split-Ring Resonator structure with cross-finger treatment, which is loaded on a microwave sensor and sequentially simulated, fabricated and measured. In order to enhance the coupling between MCSRRs, some miniaturisation is done appropriately to reduce the area of the sensor, i.e., the side slots of the MCSRRs are cross-fingered to reduce the area. The designed MCSRR sensor operates in 5.8 GHz and 8.3 GHz dual band transmission modes to sense the frequency shift. Sections II, III and IV present the design principle of the sensor, system analysis in sensing and experimental validation of the proposed sensor, respectively.

2. Sensor Design Principles

2.1. Structural Design and Simulation Analysis of Sensors

Fig.1 shows the bottom and top schematic of a microwave sensor based on a Multiple Complementary Split-Ring Resonator (MCSRR), where the orange part represents the copper foil, the yellowish part represents the dielectric plate, and the white part represents the coupling MCSRR. The dielectric plate material is Rogers RT/duriod 5880, which has a relative permittivity of 2.2 , and the dimensions of the MCSRR are 20mm*13mm*0.787mm. 0.787 mm. The MCSRR was etched on a copper ground plane (copper foil thickness 17.5 um) and used to measure the sample to be measured.

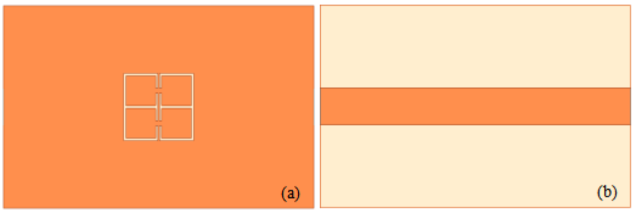

Figure 1. Schematic diagram of the cross-finger MCSRR-based sensor (a) bottom; (b) top

Based on the above information, the frequency response was modelled and simulated using HFSS software to view the frequency response, S21 The simulation results are shown in Fig.2.

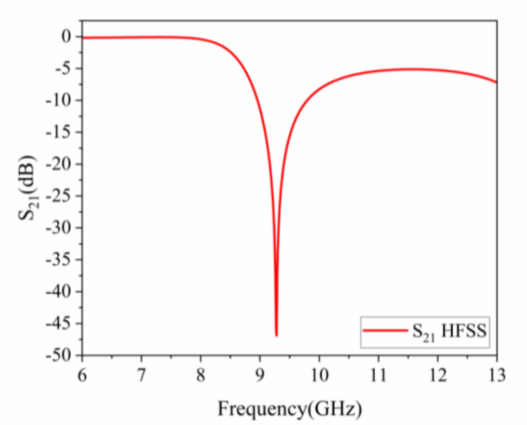

Figure 2. Scanning results based on MCSRR sensor S 21

It can be seen that the sensor operates in the 9.2 GHz band, while the sensor designed in this paper needs to operate in the 5.8 GHz band. This also indicates that there is no coupling between the two CSRR resonant units, meaning that the area of the MCSRR needs to be reduced to increase the coupling. In this case, the area is reduced by cross-fingering the side slots of the bottom MCSRR, and the schematic of the sensor with the introduction of the cross-fingering structure is shown in Fig. 3. In this case, Port 1 and Port 2 are used for input and output at both ends, respectively. The physical dimensions shown in Fig.3 are: $l = 2.2\text{mm}$, $d = 1.85mm$, $w = 0.15mm$, $g = 0.3mm$, $t = 2.36mm$.

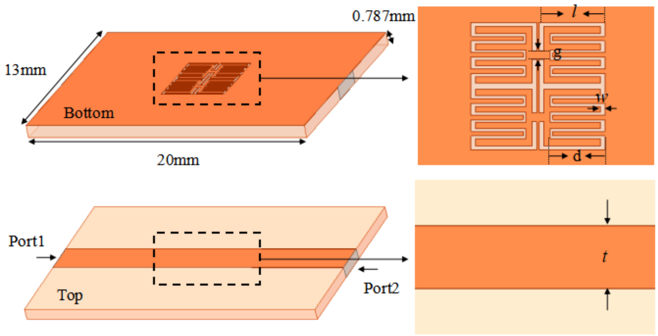

Figure 3. Schematic diagram of cross-finger MCSRR based sensor

The simulation analysis reveals that the length of the cross finger structure determines the operating frequency of the sensor. Therefore, its parameters are optimised to make it work at 5.8 GHz and the results of the parameter scan of the sensor S21 are shown in Fig.4.

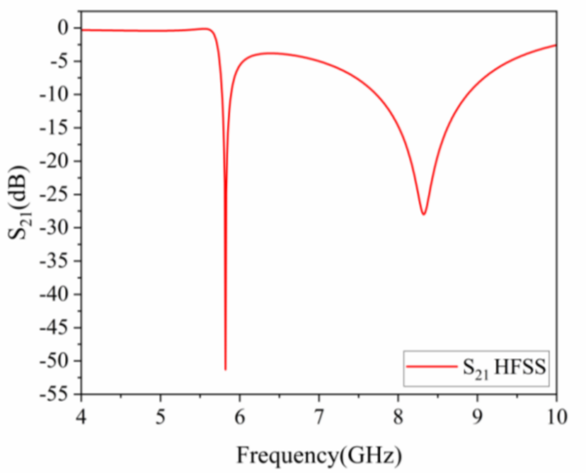

Figure 4. Scanning results based on cross-finger MCSRR sensor S 21

As can be seen from the figure, the MCSRR sensor loaded with the cross-finger processing operates in the dual-band transmission mode of 5.8 GHz and 8.3 GHz, at which time the field distribution of the sensor is shown in Fig.5.

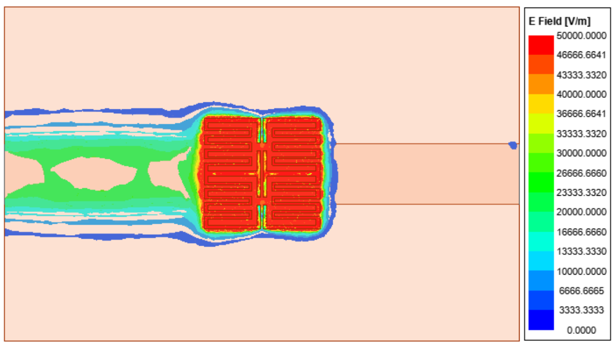

Figure 5. Electric field distribution at 5.8 GHz based on cross-finger MCSRR sensor

As can be seen from the electric field strength, there is more energy coupled to the MCSRR resonant unit, enhancing the coupling between the field and the sample to be measured.

2.2. Equivalent circuit simulation verification of the sensor

The cross-finger MCSRR-based dual-band sensor consists of two identical CSRR sensing units, which need to be close to each other in order to ensure that the sample to be tested will be loaded with a great electromagnetic field, which will stimulate its coupling ability. Fig.6 shows the equivalent circuit model of the cross-finger MCSRR-based dual-band sensor. L_r, C_r and R_r represent the equivalent inductance, capacitance and resistance of the CSRR, respectively; L_m represents the inductance of the microstrip line; C_c represents the coupling capacitance between the microstrip line and the CSRR; and C_m represents the coupling capacitance between the two CSRRs. Due to the introduction of the coupling capacitance C_m, the resonant frequency of the sensor is changed as Eq.1 :

$$f_r = \frac{f_{r0}}{\sqrt{1 - C_m/(C_r + C_c)}} \tag{1}$$

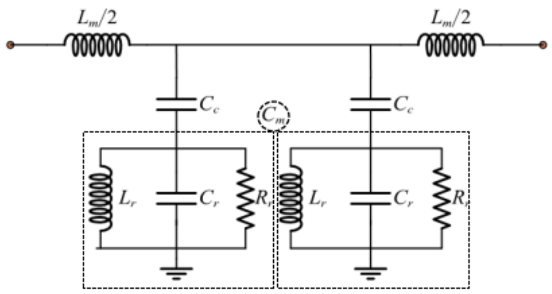

Figure 6. Equivalent circuit diagram of microstrip line loaded cross-finger MCSRR, where $L_r = 29.9\text{nH}$, the $C_r = 0.01\text{pF}$, $L_m = 2.604\text{nH}$, $C_c = 0.015\text{pF}$. $C_m = 0.0011\text{pF}$

The dielectric plate used for the sensor is Rogers RT/duriod 5880, with a relative dielectric constant of 2.2 and a thickness of 0.787 mm. In the actual equivalent circuit simulation, the coupling capacitance between the two CSRR units C_m. The inductance value within the circuit branch is 89.2465 nH, and the capacitance value is 0.003 pF. Substituting the above parameters into the ADS software for simulation, the simulation results of HFSS and ADS software are shown in Fig.7, and the electromagnetic field simulation and equivalent circuit simulation reflect very good consistency.

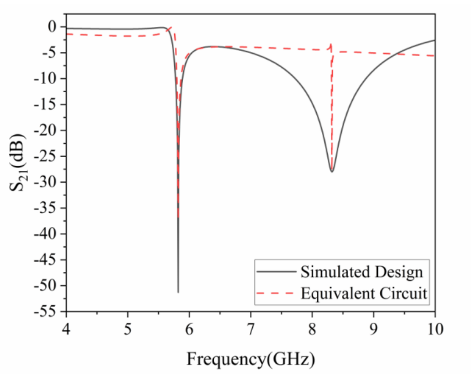

Figure 7. Cross-finger MCSRR sensor based simulation design with equivalent circuit of S21

3. Sensor System Analysis

3.1. Sensor sensitivity Analyses

The most intuitive performance indicator for measuring a sensor's dielectric constant is sensitivity, which is defined as the ratio of the change in resonant frequency to the change in dielectric constant of the sample to be measured. The formula for sensitivity (S) is:

$$S = \frac{\Delta f_r}{\Delta \varepsilon_r} \tag{2}$$

In terms of mathematical modelling, this can be specifically defined as Eq.3 :

$$S_{av,f} = \frac{f_{Empty} - f_{MUT}}{f_{Empty}(\varepsilon_r' - 1)} \times 100\% \tag{3}$$

The above equation is the normalised sensitivity expression, and f_{empty} and f_{sample} denote the resonance frequencies for the case of no load and loaded MUT of the sample to be measured, respectively.

The previous section analysed that the resonant frequency of the transducer is changed due to the addition of the coupling capacitance C_m. Then, after coupling the transducer of cross-finger MCSRR, the derivation of the capacitance C_r of Eq.4 can be obtained as

$$\frac{df_r}{dC_r} = \frac{f_{r0}}{2(C_r + C_c)[1 - C_m/(C_r + C_c)]} \tag{4}$$

It can be seen that for the addition of the coupling capacitance C_m, this structure is based on the detection of the dielectric constant, the coupling capacitance still improves the sensitivity of the resonance frequency to changes in the resonator capacitance.

The results of the above analyses are obtained through theoretical calculations, and then the sensor model is established using HFSS software based on the information of the dielectric plate and the physical dimensions of the resonator and the microstrip line. Among them, the port excitation is in the form of Wave Port, the size of which is related to the width of the microstrip line, the thickness of the dielectric plate and the copper foil; the boundary conditions of the defective copper foil ground plane (bottom) and the microstrip line (top) are set to Perfect E; the air box is used to truncate the field in the space, and the boundary condition is set to Radiation, with the size set to be greater than a quarter of the wavelength at least.

The HFSS Design model is set up with a piece of sample to be tested with dielectric constants ranging from 1 to 12 at intervals of 1, the permeability and loss tangent angle are set to 0, and the thickness is set to 1 mm, and then a parametric scanning is performed on the sample to be tested for the dielectric constants. The variation of resonant frequency with dielectric constant is obtained from the scanning, and the corresponding data are calculated by combining with Eq.3, and then imported into Origin software for fitting, and the fitted curves are shown in Fig.8.

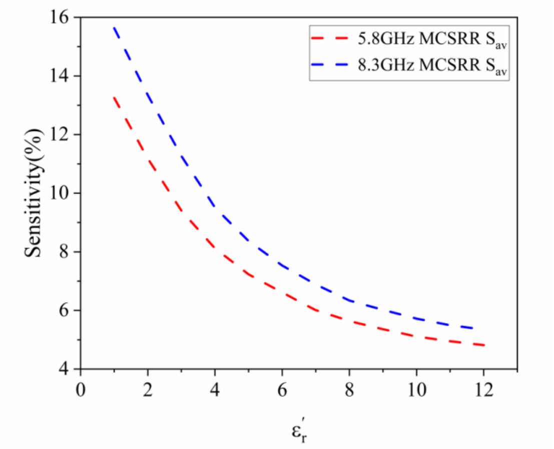

Figure 8. Fitted curves for normalised sensitivity of cross-finger MCSRR based sensors

Above, the red dashed line represents the sensitivity trend of the sensor at 5.8 GHz and the blue dashed line represents the sensitivity trend of the sensor at 8.3 GHz. The dual-band microwave sensor based on cross-fingered MCSRR shows better sensitivity than the sensors in the previous two chapters due to the cross-fingered treatment of the MCSRR's edge slots, which enhances the edge capacitance of the MCSRR.

3.2. Extraction of sensor dielectric constant

The dielectric constant of the sample to be measured is set to vary from 1 to 10 at intervals of 1 and the loss tangent is set to 0 to analyse the relationship between the resonance frequency and the variation of the dielectric constant. The variation of resonant frequency of the dual band microwave sensor based on cross finger MCSRR is shown in Fig.9:

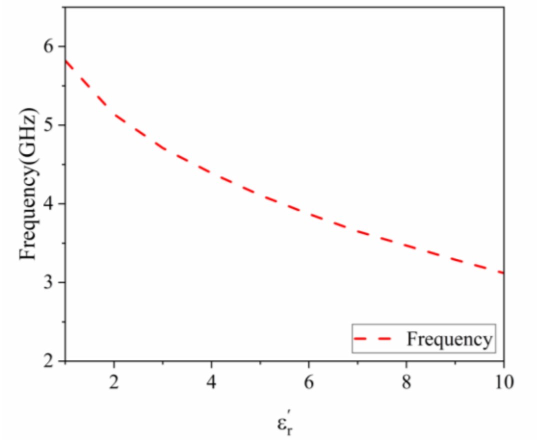

Figure 9. Curve of resonant frequency versus dielectric constant for cross-finger based MCSRR sensor

As can be seen from the figure, due to the introduction of coupling capacitance by cross-finger processing, the resonance frequency of the sample MUT to be measured still decreases with the increase of the dielectric constant, which is also in line with the change rule of the resonance frequency. Therefore, the data were fitted by Origin software, and the mathematical relationship is shown in Eq.5:

$$f_r = -3.522\varepsilon_r'^{\,0.1457} + 9.3328 \quad (5)$$

4. Sensor Fabrication Test

According to the physical dimensions in Section II, the sensor was physically fabricated on a Rogers RT/duriod 5880 dielectric substrate by photolithography of the copper foil as well as etching of the resonance ring as shown in Fig.10.The resonance region that needs to be loaded with the sample to be measured has been labelled in Fig.10 (a). The experimental measurements were carried out on a 3656B VNA with a frequency range of 4-8.5 GHz. two cables were connected to the VNA and calibrated using a 20202A 3.5 mm negative head calibration piece. After calibration, the transducer was fixed to the SMA connector (Model: SMA-KHD7) and the S21 was measured with no load , and two resonances were detected as can be clearly seen in Fig.10 (c).

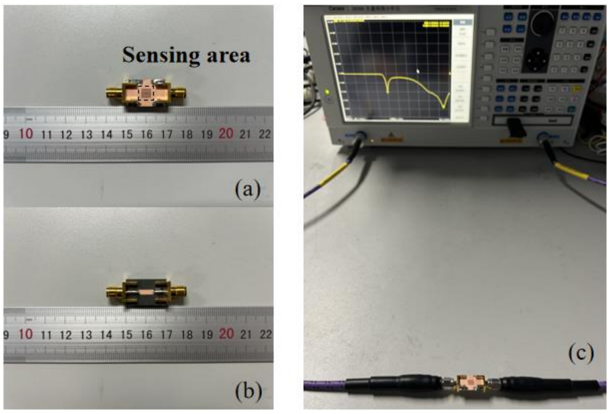

Fig. 10 Physical view of the cross-finger MCSRR-based sensor (a) bottom; (b) top;

(c) S measured by VNA at no load21

At this point, the sensor was measured in the unloaded condition and in the sensing area of the sample to be measured, respectively. Two samples to be measured were selected, Rogers RO4003 (ε_r' = 3.55, h=0.5mm) and F4BM-2 (ε_r' = 3.5, h=1mm), with uniform physical dimensions of 4.5mm*4.3mm.

Since we only focus on the measurement results at 5.8 GHz, the actual data are listed by inverting the dielectric constant through Eq.5 and compared with the results in the literature, as shown in Tab.I. In the table, the differences between the measured data and the literature data are expressed in per cent.

Table I. Comparison of measured results and literature data of dielectric constant of cross-finger MCSRR based sensor

MUT	Ref [33].	Measured Data	Different (%)
Rogers RO4003	3.55	3.89	9.58
F4BM-2	3.5	3.72	6.29

As can be seen from the table above, Rogers RO4003 and F4BM-2 samples measured better.

Error analysis:

(1) In the simulation design stage, the sensor models are constructed as ideal smooth dielectric planes to ensure that the sample to be measured is in direct contact with the resonator. However, in the actual measurement process, the smoothness of the dielectric plane is not satisfactory due to factors such as the fabrication process, resulting in a certain air gap between the sample to be measured and the resonator. This air gap is difficult to measure accurately, thus introducing a certain measurement error;

(2) In addition, external environmental factors such as air temperature and humidity may cause small perturbations to

the electromagnetic field during multiple measurements. These perturbations should not be ignored as they may have a significant impact on the measurement accuracy. Therefore, these environmental factors need to be fully considered when performing measurements and appropriate measures need to be taken to minimise their impact on the measurement results.

5. Conclusion

In this paper, a dual-band microwave sensor based on cross-fingered MCSRR dielectric constant sensitivity measurements is developed and validated, which operates in two frequency bands, 5.8 GHz and 8.3 GHz. The area is reduced by cross-fingering the side slots of the MCSRR, which enhances the coupling between the MCSRRs and results in better sensitivity. Finally, the physical fabrication of the sensor and measurement of the samples to be tested are carried out and the measured results are in accordance with the simulation results. This work verifies the feasibility of loading cross-finger MCSRR sensors.

Acknowledgments

This work was supported by the Fundamental Research Funds for the Central Universities, Southwest Minzu University, No. 2021NYYXS69.

References

[1] Veselago V G. The electrodynamic of substance with simultaneously negative values of ε and μ [J]. Soviet Physics Uspekhis, 1968,10(4): 509-514.

[2] Pendry J B, Holden A J, Robbins D J, et al. Magnetism from conductors and enhanced nonlinear phenomena [J]. IEEE Transactions on Microwave Theory and Techniques, 1999, 47(11):2075-2084.

[3] Smith D R, Padilla W J, Vier D C, et al. Composite Medium with Simultaneously Negative Permeability and Permittivity [J]. Physical Review Letters, 2000, 84(18): 4184-7.

[4] Pendry, Holden, Stewart. Extremely low frequency plasmons in metallic mesostructures [J]. Physical Review Letters, 2001, 87(11):4773-4776.

[5] Smith D R, Schurig D, Pendry J B. Negative refraction of modulated electromagnetic waves [J]. Applied Physics Letters, 2002, 81(15): 2713-2715.

[6] Lu J, Grzegorczyk T, Zhang Y, et al. Cerenkov radiation in materials with negative permittivity and permeability [J]. Optics Express, 2003, 11(7): 723-34.

[7] Qing D K, Chen G. Goos-Hänchen shifts at the interfaces between left- and right-handed media [J]. Optics Letters, 2004, 29(8): 872.

[8] Schurig D, Mock J J, Justice B J, et al. Metamaterial electromagnetic cloak at microwave frequencies [J]. Science, 2006, 314: 977-980.

[9] Falcone F, Lopetegi T, Baena J, et al. Effective negative-/spl epsiv/ stopband microstrip lines based on complementary split ring resonators [J]. IEEE Microwave and Wireless Components Letters, 2004, 14(6): 280-282 .

[10] Meng F Y, Liang Y, Wu Q , et al. Invisibility of a Metamaterial Cloak Illuminated by Spherical Electromagnetic Wave [J]. Applied Physics A, 2009, 95(3): 881~888.

[11] Tassin P, Lei Z, Th K, et al. Low-Loss Metamaterials Based On Classical Electromagnetically Induced Transparency [J]. Physical Review Letters, 2009, 102(5): 053901.

[12] Tao H, Kadlec E A, Strikwerda A C, et al. Microwave and Terahertz Wave Sensing With Metamaterials [J]. Optics express, 2011, 19(33): 21620~21626 .

[13] Horestani A K, Fumeaux C, Al-Sarawi S F, et al. Displacement Sensor Based on Diamond-Shaped Tapered Split Ring Resonator [J]. IEEE Sensors Journal, 2013, 13(4): 1153-60.

[14] Collette C, Fueyo R, Horodinca M, et al. Prototype of a small low noise absolute displacement sensor [J]. IEEE Sensors Journal, 2014, 14(1): 91-95.

[15] Horestani A K, Naqui J, Abbott D, et al. Two-dimensional displacement and alignment sensor based on reflection coefficients of open microstrip lines loaded with split ring resonators [J]. Electronics Letters, 2014, 50(8): 620-2.

[16] Horestani A K, Naqui J, Shaterian Z, et al. Two-dimensional alignment and displacement sensor based on movable broadside-coupled split ring resonators [J]. Sensors and Actuators A: Physical, 2014, 210: 18-24.

[17] Tian Ying. Research and design of metamaterial sensor based on open-slit ring resonator [D]. Central China Normal University, 2018.

[18] Lee C-S, Yang C-L. Complementary Split-Ring Resonators for Measuring Dielectric Constants and Loss Tangents [J]. IEEE Microwave and Wireless Components Letters, 2014, 24(8): 563-5.

[19] Galindo-Romera G, Herraiz-Martínez F J, Gil M, et al. Submersible Printed Split Ring Resonator-Based Sensor for Thin-Film Detection and Permittivity Characterisation [J]. IEEE Sensors Journal, 2016, 16(10): 3587-96.

[20] Hu Pepe. Theoretical and experimental study of CSRR characteristics [D]. North China Electric Power University, 2019.

[21] Albishi A M, Badawe M K E, Nayyeri V, et al. Enhancing the Sensitivity of Dielectric Sensors With Multiple Coupled Complementary Split-Ring Resonators [J]. IEEE Transactions on Microwave Theory and Techniques, 2020, 68(10): 4340-7.

[22] Zhang ZY. Research on the application of metamaterials in microwave dielectric constant sensors [D]. Jilin University, 2022.

[23] Singh S K, Tiwari N K, Yadav A K, et al. Design of ZnO/N-Doped Graphene Nanohybrid Incorporated RF Complementary Split Ring Resonator Sensor for Ammonia Gas Detection [J]. IEEE Sensors Journal, 2019, 19(18): 7968-75.

[24] Kiani S, Rezaei P, Navaei M. Dual-sensing and dual-frequency microwave SRR sensor for liquid samples permittivity detection [J]. MEASUREMENT, 2020, 160.

[25] Javadian-Saraf A, Hosseini E, Daniel Wiltshire B, et al. Graphene oxide/polyaniline-based microwave split-ring resonator: a versatile platform towards ammonia sensing [J]. Journal of Hazardous Materials, 2021, 418.

[26] Gan Hongyi. Design of high-performance and miniaturised planar microwave sensor based on complementary open resonant ring (CSRR)[D]. Hangzhou University of Electronic Science and Technology, 2021.

[27] Wang, D. X.. Research and design of dielectric constant test method based on resonant characteristics of microwave structures[D]. Chongqing University of Posts and Telecommunications, 2021.

[28] Li Yao. Research on pulse wave velocity measurement based on complementary open-ring resonator[D]. Dalian University of Technology, 2022.

[29] Hairong K, Libo Y, Xiaoyong Z, et al. Wireless Passive Microwave Antenna-Integrated Temperature Sensor Based on CSRR. [J]. Micromachines, 2022, 13(621): 1-10.

[30] Mohammed M, Bait S, et al. Detection of Reinforced Concrete Blocks Using Two-Port Microwave CSRR Sensor.[J]. IEEE Access, 2022, 10: 89437-89444 .

[31] Zizhuo S, Huixin Z, Shaojun Z, et al. A Microwave CSRR Sensor for Non-Invasive Glucose-Level Detection. [J]. IEEE 5th International Conference on Electronic Information and Communication Technology (ICEICT), 2022, 872-874.

[32] Hong X, Sen Y, Cheng G, et al. A Dual-Scale CSRRs-Based Sensor for Dielectric Characterisation of Solid Materials. [J]. IEEE Sensors Council, 2022, 3502704.

[33] Xiaoming L, Dan Z, Shuo Y, et al. A Dual-Band Resonator Sensor for Low Permittivity Characterisation. [J]. IEEE Transactions on Instrumentation and Measurement, 2022, 71: 8006511.